THE JOURNAL OF PHYSICAL CHEMISTRY C

Article

pubs.acs.org/JPCC

Solvate Structures and Computational/Spectroscopic Characterization of Lithium Difluoro(oxalato)borate (LiDFOB) Electrolytes

Sang-Don Han,[†] Joshua L. Allen,[†] Erlendur Jónsson,[‡] Patrik Johansson,[‡] Dennis W. McOwen,[†] Paul D. Boyle,[§] and Wesley A. Henderson*[,†]

[†]Ionic Liquids & Electrolytes for Energy Technologies (ILEET) Laboratory, Department of Chemical & Biomolecular Engineering, North Carolina State University, Raleigh, North Carolina 27695, United States

[‡]Department of Applied Physics, Chalmers University of Technology, SE-412 96, Gothenburg, Sweden

[§]X-ray Structural Facility, Department of Chemistry, North Carolina State University, Raleigh, North Carolina 27695, United States

Supporting Information

ABSTRACT: Lithium difluoro(oxalato)borate (LiDFOB) is a relatively new salt designed for battery electrolyte usage. Limited information is currently available, however, regarding the ionic interactions of this salt (i.e., solvate formation) when it is dissolved in aprotic solvents. Vibrational spectroscopy is a particularly useful tool for identifying these interactions, but only if the vibrational bands can be correctly linked to specific forms of anion coordination. Single crystal structures of LiDFOB solvates have therefore been used to both explore the $DFOB^-$...Li^+ cation coordination interactions and serve as unambiguous models for the assignment of the Raman vibrational bands. The solvate crystal structures determined include $(monoglyme)_2$:LiDFOB, $(1,2\text{-diethoxyethane})_{3/2}$:LiDFOB, $(acetonitrile)_3$:LiDFOB, $(acetonitrile)_1$:LiDFOB, $(dimethyl\ carbonate)_{3/2}$:LiDFOB, $(succinonitrile)_1$:LiDFOB, $(adiponitrile)_1$:LiDFOB, $(PMDETA)_1$:LiDFOB, $(CRYPT\text{-}222)_{2/3}$:LiDFOB, and $(propylene\ carbonate)_1$:LiDFOB. DFT calculations have been incorporated to provide additional insight into the origin (i.e., vibrational modes) of the Raman vibrational bands to aid in the interpretation of the experimental analysis.

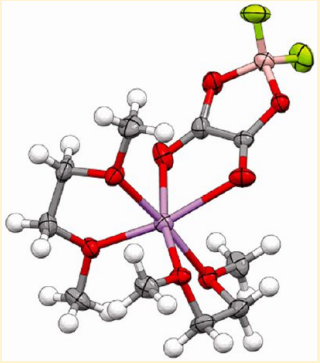

1. INTRODUCTION

The difluoro(oxalato)borate ($DFOB^-$) anion, also known as oxalyldifluoroborate ($ODFB^-$), was first reported in a patent application filed in 1999 by Metallgesellschaft AG[1] and in a publication in 2006 by the U.S. Army Research Laboratory (ARL).[2] The lithium salt with this anion (LiDFOB) has garnered significant interest in recent years for Li-ion battery electrolytes.[3−39] Little is known at present, however, about the molecular-level ionic interactions present once this salt is dissolved in the aprotic solvents used for electrolytes. Such knowledge is necessary to understand the origin of electrolyte properties as solvent−salt mixtures consist of a diverse range of solvate species.[40,41]

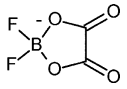

The solvates present in electrolytes may be broadly classified as solvent-separated ion pair (SSIP), contact ion pair (CIP) or aggregate (AGG) solvates if the anions are coordinated to zero, one or more than one Li^+ cation, respectively. Vibrational spectroscopy (Raman, FTIR) is the predominant means for determine the extent of ionic association in electrolytes by examining the variation in anion vibrational band positions. When an anion forms one or more coordination bonds to Li^+ cations, the anion electron density distribution (and thus bond lengths and angles) changes, leading to vibrational band variation. For Raman spectroscopy, the variability of the solvate species present in solution, however, typically results in broad overlapping anion Raman bands which can be difficult to deconvolute correctly and thus properly interpret to distinguish the specific forms of anion...Li^+ cation coordination. Computational methods may be utilized to assign the band positions for varying forms of coordination.[42−46] Unfortunately, such studies, while extremely useful for understanding the anion vibrational bands, do not always provide a definitive validation for the assignments. It has previously been demonstrated, however, that crystalline solvates with known structures can be utilized as models for the spectroscopic characterization of different forms of ClO_4^-...Li^+ cation coordination.[47−52] These analyses are of particular relevance as they indicate that many of the vibrational assignments previously published for the coordination found in $LiClO_4$-based electrolytes are either incorrect or oversimplifications of the true ionic association state present in the electrolytes.

Received: September 13, 2012
Revised: February 1, 2013
Published: February 5, 2013

Although useful for discussions, the general classification of SSIP, CIP, and AGG solvates fails to fully account for the coordination complexity that may exist. This classification must therefore be further differentiated to include specific forms of anion coordination, examples of which are shown in Chart 1 for

Chart 1. $DFOB^-$...Li^+ Cation Coordination: (a) SSIP, (b) CIP-I, (c) CIP-II, (d) AGG-Ia, (e) AGG-Ib, (f) AGG-Ic, (g) AGG-Id, (h) AGG-IIa, (i) AGG-IIb, (j) AGG-IIIa, and (k) AGG-IIIb[a]

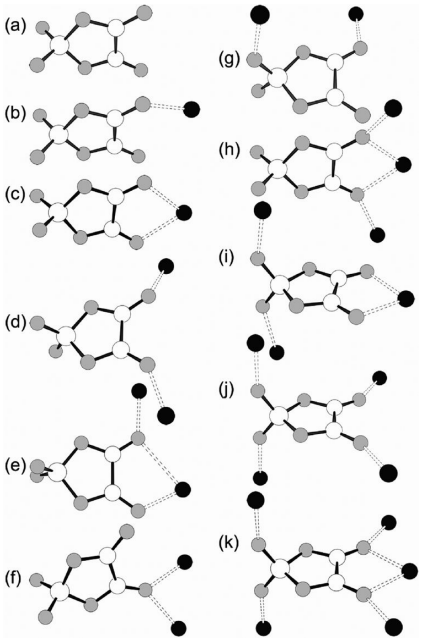

[a]Other forms of coordination may also occur. Li^+ cations are colored black.

the $DFOB^-$ anion. Each of these different forms of coordination results in a different vibrational spectral fingerprint. To explore this in depth, the crystal structures for ten new crystalline solvate structures with LiDFOB are reported here. The Raman spectroscopic characterization of these solvates is also provided, as well as the data for the salt LiDFOB and other LiDFOB solvates for which a structure is known or can be reasonably presumed. In addition, density functional theory (DFT) calculations for the uncoordinated (i.e., SSIP) $DFOB^-$ anion and the CIP-II (Chart 1) form of $DFOB^-$...Li^+ cation coordination are presented to elucidate the vibrational modes which contribute to the vibrational bands and their correlation with the spectra for the crystalline solvates.

2. EXPERIMENTAL SECTION

2.1. Materials. LiDFOB was synthesized by the direct reaction of excess boron trifluoride diethyl etherate (BF_3-ether) with lithium oxalate (oxalic acid dilithium salt), both used as-received from Sigma-Aldrich. The resulting salt was extracted/recrystallized several times from dimethyl carbonate (DMC) as a $(DMC)_{3/2}$:LiDFOB crystalline solvate. This solvate was subsequently vacuum-dried at 105 °C for 48 h, yielding the high purity anhydrous LiDFOB salt free of solvent.[11]

The solvents used in the present study and their acronyms are noted in Chart 2. The ethylene glycol dimethyl ether or 1,2-dimethoxyethane (monoglyme or G1, anhydrous, 99.5%), diethylene glycol dimethyl ether or 2-methoxyethyl ether

Chart 2. Structures and Acronyms of the Solvents Studied

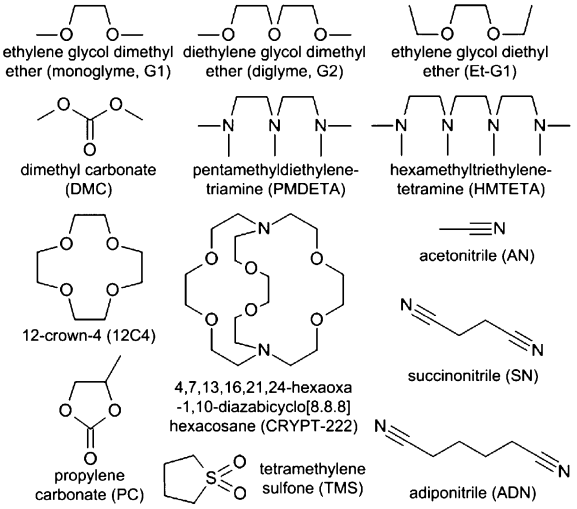

(diglyme or G2, anhydrous, 99.5%), ethylene glycol diethyl ether or 1,2-diethoxyethane (Et-G1, 98%), *N*,*N*,*N*′,*N*″,*N*″-pentamethyldiethylenetriamine (PMDETA, 99%), 1,1,4,7,10,10-hexamethyltriethylenetetramine (HMTETA, 97%), 1,4,7,10-tetraoxacyclododecane (12-crown-4 or 12C4, 98%), 4,7,13,16,21,24-hexaoxa-1,10-diazabicyclo[8.8.8]-hexacosane (CRYPT-222, 98%), acetonitrile (AN, extra dry, 99.9%), succinonitrile (SN, 99%), adiponitrile (ADN, 99%), tetramethylene sulfone or sulfolane (TMS, 99%), propylene carbonate (PC, anhydrous, 99.7%) and dimethyl carbonate (DMC, anhydrous, ≥ 99%) were purchased from either Fisher Scientific or Sigma-Aldrich and used as-received. The water content of the solvents was verified to be negligible (<30 ppm) using a Mettler Toledo DL39 Karl Fischer coulometer. The materials were handled and stored in a Vacuum Atmospheres inert atmosphere (N_2) glovebox (<1 ppm H_2O).

2.2. Sample Preparation. Mixtures were prepared in the glovebox by combining appropriate amounts of LiDFOB with solvents in hermetically-sealed glass vials which were then heated and stirred on a hot plate until the salt fully dissolved. Compositions were typically slightly more dilute than the solvate composition of interest. Single crystals grew from the mixtures upon standing either at room temperature, at 4 °C (in a refrigerator), at −23 °C (in a freezer) or at −20 °C to −40 °C (in a Binder environmental chamber). Single crystals were used both for the determination of the structures via single-crystal X-ray diffraction and for the Raman analysis by grinding the crystals in the glovebox using a mortar and pestle (if the melting point (T_m) of the solvate is greater than room temperature). If the solvates melt at or below room temperature, then liquid samples of the appropriate composition were instead prepared in the glovebox and the samples were crystallized directly in the Linkam heating/cooling stage during the Raman measurements (note that this sometimes produces large crystals for which orientational effects impact the Raman peak intensities).

2.3. Solvate Crystal Structure Determination. Samples were mounted on nylon loops with a small amount of Paratone N oil. X-ray measurements were made on a Bruker-Nonius Kappa Axis X8 Apex2 diffractometer. The unit cell dimensions were determined from symmetry constrained fits of the reflections. The frame integrations were performed using SAINT.[53] The resulting raw data were scaled and absorption

dx.doi.org/10.1021/jp309102c | J. Phys. Chem. C 2013, 117, 5521−5531

corrected using a multiscan averaging of symmetry equivalent data using SADABS.[54] The structures were solved by direct methods using the SIR92[54] or XS[55] programs. All non-hydrogen atoms were obtained from the initial solution. The hydrogen atoms were introduced at idealized positions and were allowed to ride on the parent atom. The structural models were fit to the data using full matrix least-squares based on F^2. The calculated structure factors included corrections for anomalous dispersion from the usual tabulation. The structures were refined using the XL program from SHELXTL.[55] Additional details are available in the Supporting Information (SI). Structures were drawn using Ortep-3 or Mercury 3.0 software. Crystallographic information data files (CIFs) for the solvates are available in the SI and free of charge from the Cambridge Crystallographic Data Centre via www.ccdc.cam.ac.uk/data_request/cif: CCDC 896911 $(ADN)_1$:LiDFOB, 896912 $(AN)_1$:LiDFOB, 896913 $(AN)_3$:LiDFOB, 896914 $(CRYPT\text{-}222)_{2/3}$:LiDFOB, 896915 $(DMC)_{3/2}$:LiDFOB, 896916 $(Et\text{-}G1)_{3/2}$:LiDFOB, 896917 $(G1)_2$:LiDFOB, 896918 $(PC)_1$:LiDFOB, 896919 $(PMDETA)_1$:LiDFOB and 896920 $(SN)_1$:LiDFOB. Mercury freeware software to view the content of these files is available: www.ccdc.cam.ac.uk/free_services/mercury/downloads/.

2.4. Elemental Analysis. The analysis of crystals for the $(12C4)_2$:LiDFOB and $(HMTETA)_1$:LiDFOB solvates was performed by Atlantic Microlab, Inc.—$C_{18}H_{32}O_{12}F_2BLi$ for $(12C4)_2$:LiDFOB, calcd: C 43.57, F 7.66, H 6.50; found: C 43.50, F 7.53, H 6.36 and $C_{14}H_{34}O_4F_2BLiN_4$ for $(HMTETA)_1$:LiDFOB, calcd: C 44.46, N 14.81, F 10.05 H 9.06; found: C 44.45, N 14.78, F 9.86, H 8.39—confirming these as the correct compositions. A similar analysis was not performed on crystals for the $(G2)_2$:LiDFOB solvate as this solvate melts below ambient temperature (SI).

2.5. Raman Spectroscopy. Raman vibrational spectra were collected with a Horiba-Jobin Yvon LabRAM HR VIS high resolution confocal Raman microscope using a 632 nm He−Ne laser as the exciting source and a Linkam stage for temperature control with a long distance 50× objective. An elemental Si reference (520.7 cm^{-1}) was used for spectral axis calibration. The zero position of the laser line and the Si line position were aligned prior to the data collection for each sample. The samples were hermetically-sealed in the Linkam stage in the glovebox before transferring the stage to the spectrometer. Spectra were typically collected using a 20 s measurement time with 10 accumulations. The samples were cooled/heated at 5 °C min^{-1} and the spectra were collected from −100 to 60 °C at intervals of 20 °C. Raman spectra were processed using LabSpec software.

2.6. Computational Details. The $DFOB^-$ anion and its various ion pairs with a Li^+ cation were constructed manually and geometry optimized using the 6-311+G* basis set employing two different DFT functionals: B3LYP[56−58] and M06−2X[59]—the former to support backward compatibility (significant previous work has been done using only the B3LYP functional) and the latter to make use of the recent development of better functionals (M06−2X). Utilizing both serves as an internal calibration/verification of the results. Subsequently, the structures were all verified as energy minima by computing their Hessians and the Raman spectral data (frequencies, activities) were obtained from the partial third derivatives of the energy. In addition to the above calculations, all done for ionic species in vacuum, a solvent effect was added (with the structures reoptimized) using a solvent self-consistent reaction field (SCRF-SMD) methodology[60] with AN as the parametrized solvent. This was done to in some way account for the reduced ion−ion interactions in the crystalline and/or liquid environment, and thus to mimic the experimental analysis to some extent. As the $DFOB^-$ anion is able to adopt a multitude of different forms of Li^+ cation coordination, the same strategy as noted above was also employed to scrutinize various ion pairs for numerous $DFOB^-$...Li^+ cation combinations. All calculations were made using Gaussian 09.[61] To assist the comparison with the experimental data, artificial Raman spectra were created by convolution of the spectral data using a Lorentzian band shape and a fwhm of 5 cm^{-1}.

3. RESULTS AND DISCUSSION

Although vibrational spectroscopy is a powerful tool for delineating the anion interactions with Li^+ cations, limitations exist for transcribing such information into a robust understanding of the ionic association interactions in solution. This is evident from a scrutiny of the solvate crystal structures. Figure 1 shows examples of two different forms of anion CIP

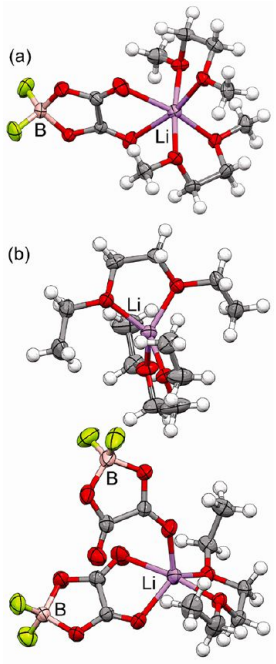

Figure 1. $DFOB^-$...Li^+ cation coordination in the crystalline solvates: (a) $(G1)_2$:LiDFOB and (b) $(Et\text{-}G1)_{3/2}$:LiDFOB (Li-purple, O-red, B-tan, F-light green).

coordination in the $(G1)_2$:LiDFOB and $(Et\text{-}G1)_{3/2}$:LiDFOB crystalline solvates. Vibrational spectroscopy only indirectly provides information about the Li^+ cation interactions. Thus, for the $(Et\text{-}G1)_{3/2}$:LiDFOB crystalline solvate, the spectroscopic data would indicate a mixture of CIP-I and CIP-II solvates. But, from the perspective of the Li^+ cation coordination, the structure instead consists of SSIP and AGG solvates. Similarly, the spectroscopic data for the $(CRYPT\text{-}222)_{2/3}$:LiDFOB solvate correspond to CIP-I/CIP-II/AGG-Id coordination (three symmetrically independent anions), whereas the Li^+ cation coordination is SSIP/SSIP/AGG. Molecular dynamics (MD) simulations of electrolyte mixtures point to a further complexity. In the liquid mixtures, there is a distribution of fully solvated Li^+ cations and uncoordinated anions, ion pairs

dx.doi.org/10.1021/jp309102c | J. Phys. Chem. C 2013, 117, 5521−5531

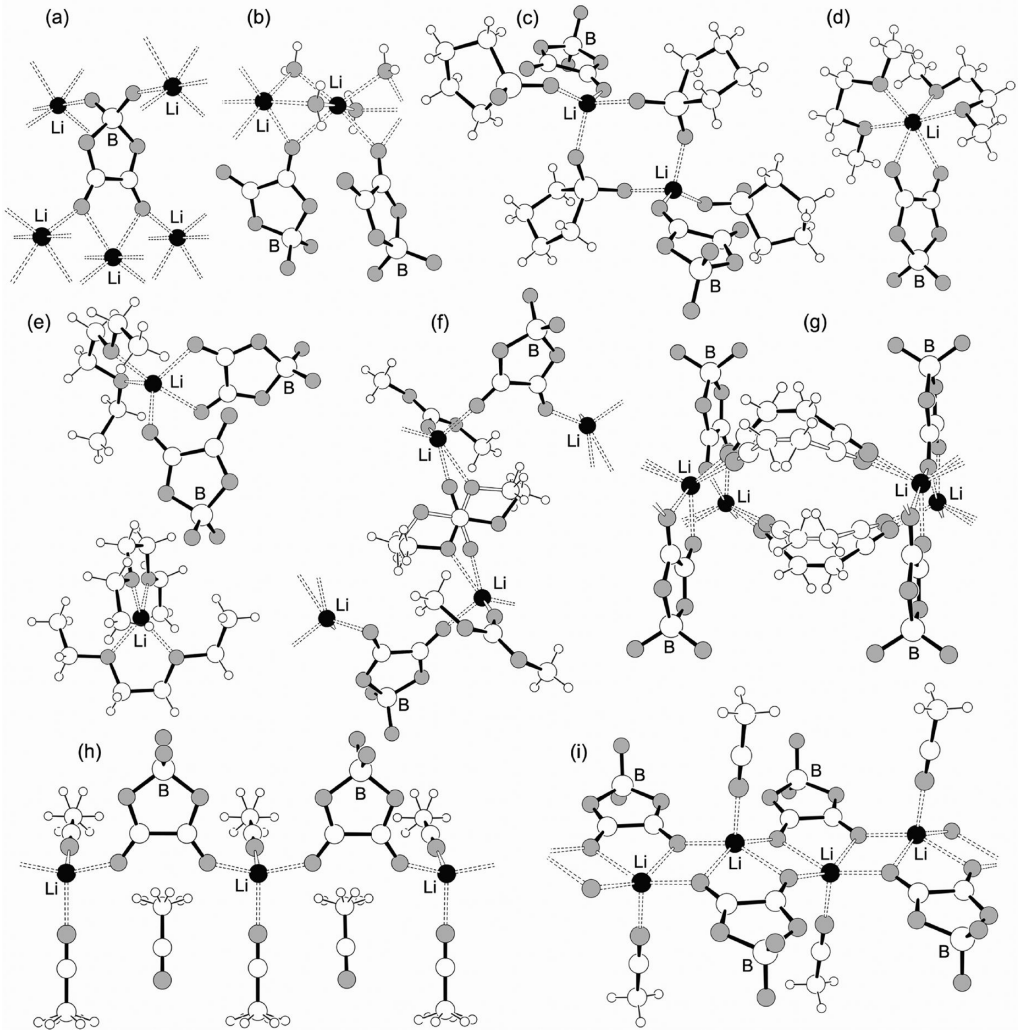

Figure 2. $DFOB^-$...Li^+ cation coordination in crystalline LiDFOB and the crystalline solvates studied: (a) AGG-IIIb LiDFOB,[11] (b) AGG-Ic $(H_2O)_1$:LiDFOB,[11] (c) CIP-I $(TMS)_2$:LiDFOB,[16] (d) CIP-II $(G1)_2$:LiDFOB, (e) CIP-I/CIP-II $(Et\text{-}G1)_{3/2}$:LiDFOB, (f) AGG-Ia $(DMC)_{3/2}$:LiDFOB, (g) AGG-Ib $(SN)_1$:LiDFOB, (h) AGG-Ia $(AN)_3$:LiDFOB, and (i) AGG-IIa $(AN)_1$:LiDFOB.

and aggregate clusters of ions which may be present.[40,41] These solvated aggregate clusters may contain one or more anions coordination to one Li^+ cation (i.e., CIP coordination), but the cluster itself may actually be quite large with many ions (i.e., the Li^+ cation may be bonded to additional anions).[40] Thus, the spectroscopic data may again not be indicative of the true state of ionic association. Caution should therefore be exercised in directly translating the information obtained from a spectral analysis of electrolytes into an interpretation of solvate distribution as doing so may be highly misleading. Considerable insight from such an analysis may be obtained, however, when the spectroscopic data are used in tandem with other methods.[40,41]

3.1. Solvate Structures and Li^+ Cation Coordination. Figures 2 and 3 show schematic illustrations of the $DFOB^-$...Li^+ cation coordination in the crystalline solvates. The structures for pure LiDFOB, $(H_2O)_1$:LiDFOB and $(TMS)_2$:LiDFOB have been previously reported.[11,16] The remaining structures were determined as part of the present study (SI). The $DFOB^-$ anion is able to adopt a multitude of different forms of Li^+ cation coordination. All of the anions in the solvate structures have at least one of the carbonyl oxygen atoms coordinated to a Li^+ cation. The two carbonyl oxygen atoms may coordinate up to three Li^+ cations using the four electron lone-pairs available. Bidentate coordination of a Li^+ cation by both carbonyl oxygen atoms is found in seven of the structures: LiDFOB, $(G1)_2$:LiDFOB, $(Et\text{-}G1)_{3/2}$:LiDFOB, $(ADN)_1$:LiDFOB, $(SN)_1$:LiDFOB, $(AN)_1$:LiDFOB and $(CRYPT\text{-}222)_{2/3}$:LiDFOB. This suggests that this is a common feature for the anion...Li^+ cation interactions in the solid-state structures. Other anions such as bis(oxalatoborate) (BOB^-),[44] dicyanotriazolate ($DCTA^-$ or $TADC^-$)[45] and bis(trifluoromethanesulfonyl)imide ($TFSI^-$)[41] may also have a tendency to form bidentate coordination, but this appears to diverge from the behavior of anions such as ClO_4^-, BF_4^-, and PF_6^-, which instead typically coordinate Li^+ cation in solid-state solvate structures and in solution (the latter from MD simulations) via monodentate coordination.[50,62] Only four of the structures contain Li^+ cations coordinated by fluorine atoms: LiDFOB, $(ADN)_1$:LiDFOB, $(CRYPT\text{-}222)_{2/3}$:LiDFOB and $(PC)_1$:LiDFOB. In all of these solvates, the fluorine atom coordination serves as a necessary bridge to weld the structure together. This suggests that while fluorine atom coordination to Li^+ cations may occur, it is much less prevalent than the carbonyl oxygen atom coordination.

dx.doi.org/10.1021/jp309102c | J. Phys. Chem. C 2013, 117, 5521−5531

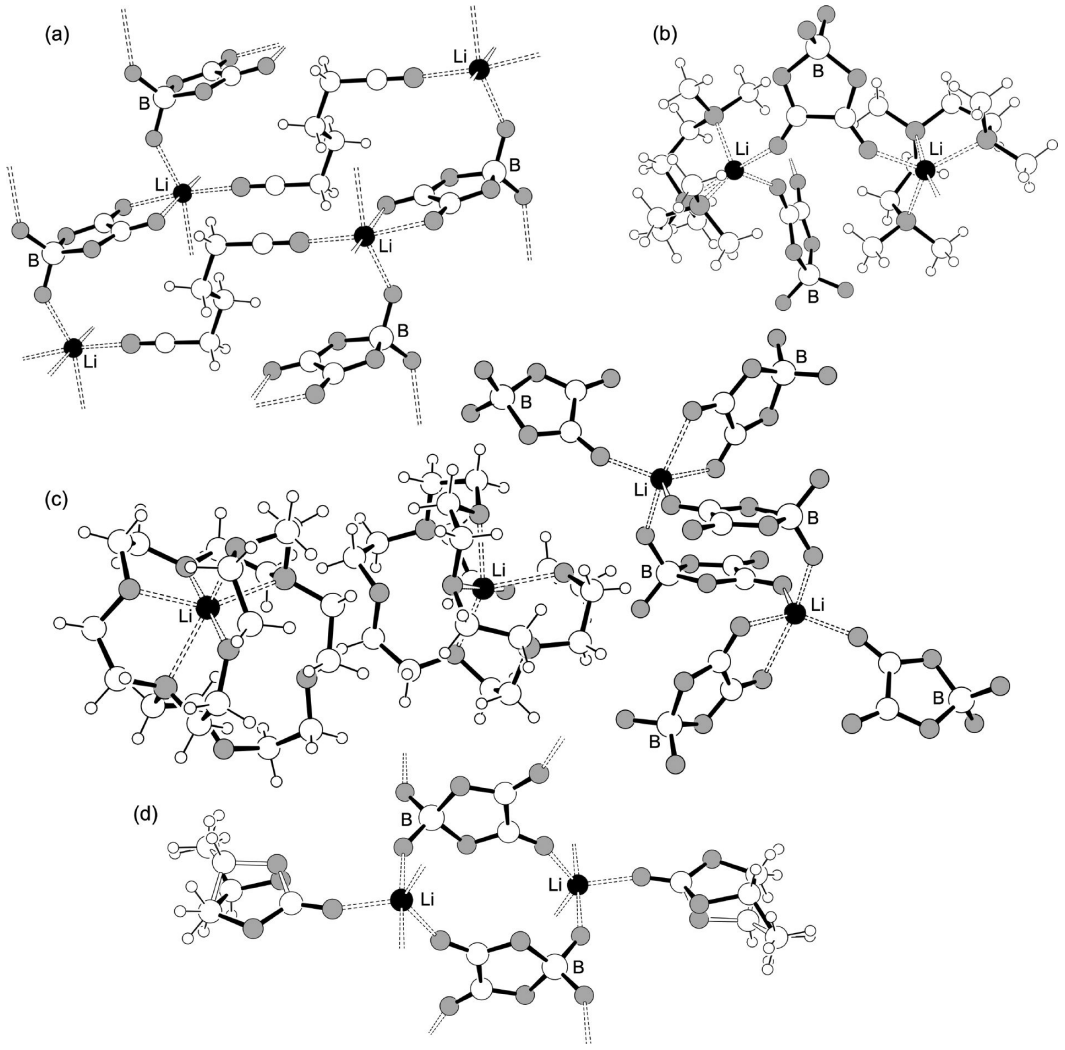

Figure 3. $DFOB^-$...Li^+ cation coordination in the crystalline solvates studied: (a) AGG-IIb $(ADN)_1$:LiDFOB, (b) AGG-Ia $(PMDETA)_1$:LiDFOB, (c) CIP-I/CIP-II/AGG-Id $(CRYPT\text{-}222)_{2/3}$:LiDFOB, and (d) AGG-IIIa $(PC)_1$:LiDFOB.

3.2. Raman Band Assignments. The experimental Raman spectrum for the anhydrous LiDFOB crystalline salt is shown in Figure 4. To aid in the assignment of the peaks, the DFT computed vibrational modes for the uncoordinated $DFOB^-$ anion are shown in Table 1. Note that differences are to be expected between the spectra for the anions in the highly aggregated salt and the uncoordinated anions. The vibrational modes may be visualized (through animation) using the Gaussian 09 output files (.xyz format) and instructions provided in the SI.

The two strong peaks found above 1700 cm^{-1} in Figure 4 correspond to the C═O stretching vibrations—antisymmetric and symmetric, respectively (Table 1 and Chart 3 which note that the DFT calculations predict too high a frequency for these by ~100 cm^{-1}). Judging from the structural data, these bands should be excellent probes for the $DFOB^-$...Li^+ cation interactions as these occur principally via the anion carbonyl groups. This was found, however, not to be the case. A summary of the symmetric C═O stretching band positions for the crystalline solvates is given in the SI. In contrast to expectations, this analysis suggests that the band positions for these $DFOB^-$ anion carbonyl vibrational modes do not enable the facile discrimination of the different forms of anion coordination.

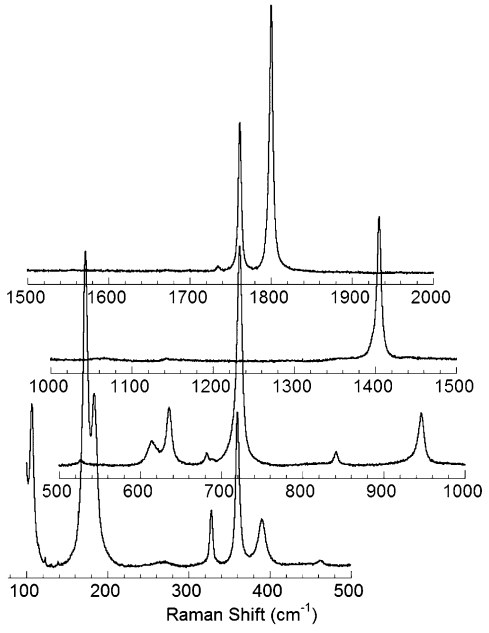

Figure 4. Raman spectrum of LiDFOB (at 20 °C).

dx.doi.org/10.1021/jp309102c | J. Phys. Chem. C 2013, 117, 5521−5531

Table 1. Calculated (Uncoordinated DFOB$^-$ from M06-2X) Vibration Mode Frequencies (cm^{-1}), Raman Activities (Å^4 amu^{-1}) and IR Intensities (km mol^{-1}), and Tentative Assignments (No Scaling)[a]

	vacuum			SMD			
freq$_{expt}$	freq	I_{Raman}	I_{IR}	freq	I_{Raman}	I_{IR}	tentative assignments
	81	1.61	2.10	82	2.55	2.53	B centered torsion
	114	0.72	0	110	1.09	0	torsion of O═C−C═O + ring + F−B−F
325	331	0.28	∼0	328	0.38	∼0	ring twisting + torsion of F−B−F
360	334	2.22	0.09	338	3.46	0.63	symm bend O═C−O in-plane + F−B−F bend out-of-phase
390	363	1.60	11.49	365	2.55	25.11	symm bend O═C−O in-plane + F−B−F bend in-phase
	373	0.05	7.34	371	0.06	15.52	∂(C−C) + π(F−B)
	468	0.12	19.63	467	0.42	33.07	π symm C−C
	522	0.30	25.05	517	0.44	40.49	∂(O═C−O) × 2 + ρ rock B−F
615	605	2.24	14.92	608	3.15	19.20	∂(O−C−C)
635	621	2.33	0.68	619	3.85	1.00	B−F scissoring + O−B symm bend
680	690	0.44	2.78	695	0.96	2.95	ring rotation
723	728	9.55	7.41	739	15.53	9.95	ring breathing
840	856	0.53	∼0	854	1.25	0.01	bend C−C (out of plane) + displacements of O
942	957	2.82	0.49	964	5.33	2.10	symm B−O stretch + C−C stretch + B−F stetch
	987	0.04	240.71	989	0.14	358.15	antisymm B−O stretch
	1119	0.30	785.88	1078	0.63	1288.27	symm B−F stretch
	1177	0.29	382.10	1113	0.47	534.47	antisymm B−F stretch
	1290	0.01	197.31	1278	0.18	264.56	in-plane C−C bending + antisymm C−O stretch
1405	1397	6.39	478.92	1386	7.61	677.46	symm C−O stretch + C−C stretch
1769	1870	13.75	172.05	1865	25.17	223.30	antisymm C═O stretch
1800	1906	19.19	713.11	1900	45.02	912.41	symm C═O stretch

[a]The term freq$_{expt}$ refers to the LiDFOB salt (Figure 4).

Chart 3. Principal Bonds/Angles Contributing to the DFOB$^-$ Anion Vibrational Modes as Determined from DFT Calculations (See SI)

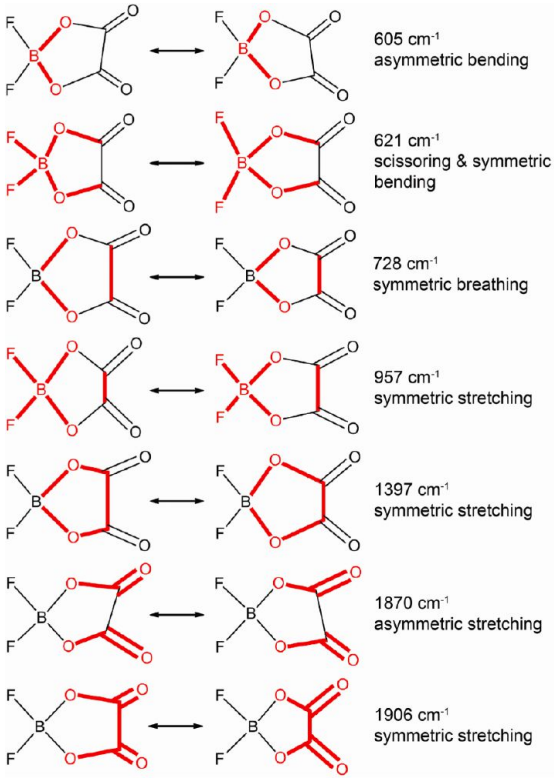

The peak observed at 1405 cm^{-1} (Figure 4) is attributed to the combination band of the C−C and symmetric C−O stretching modes (Table 1 and Chart 3). The peak near 942 cm^{-1} (Figure 4) corresponds to a combination of symmetric B−O, C−C, and B−F stretching modes (Table 1 and Chart 3). The very strong peak near 723 cm^{-1} (Figure 4), predicted by the computations to be the third strongest peak in the Raman spectra, is due to a ring-breathing mode (Table 1 and Chart 3). The more complex modes corresponding to the two or more peaks observed at ∼600−620 cm^{-1} (Figure 4) are most likely a combination of different O−C−C bending modes, but combined also with B−F scissoring from the other half of the DFOB$^-$ anion (Table 1 and Chart 3). Thus, this region is more difficult to use as a probe for specific DFOB$^-$...Li$^+$ cation interactions. Yet, this should, at the same time, be the region with bands which undergo a sizable shift in position due to any Li$^+$...anion fluorine atom coordination. It is important to also note that boron isotopes have a natural abundance of 19.9% ^{10}B and 80.1% ^{11}B. Thus, vibrational modes which involve the displacement of the boron nucleus will give two different bands. This adds a further level of complexity to the band analysis for the DFOB$^-$ anion.

3.3. Raman Spectroscopic Analysis of Crystalline Solvates. The majority of the solvates with known crystal structures were characterized by Raman spectroscopy to determine the anion band position variation with varying coordination and temperature. The AGG-Ic $(H_2O)_1$:LiDFOB solvate, however, was not analyzed as this solvate contains significant hydrogen bonding between the water and anions (which is expected to perturb the vibrational bands), nor was the CIP-I/CIP-II/AGG-Id $(CRYPT\text{-}222)_{2/3}$:LiDFOB solvate analyzed as the crystals melt below ambient temperature and it was not possible to prepare the correct liquid composition (i.e., dissolve the appropriate amount of LiDFOB salt directly in the solvent). Unfortunately, the anion bands near 945 and 1405 cm^{-1} overlap significantly with the peaks from many common solvents. The bands in the 600−650, 705−725, and 1780−1820 cm^{-1} region of the spectra, however, do not and these bands

dx.doi.org/10.1021/jp309102c | J. Phys. Chem. C 2013, 117, 5521−5531

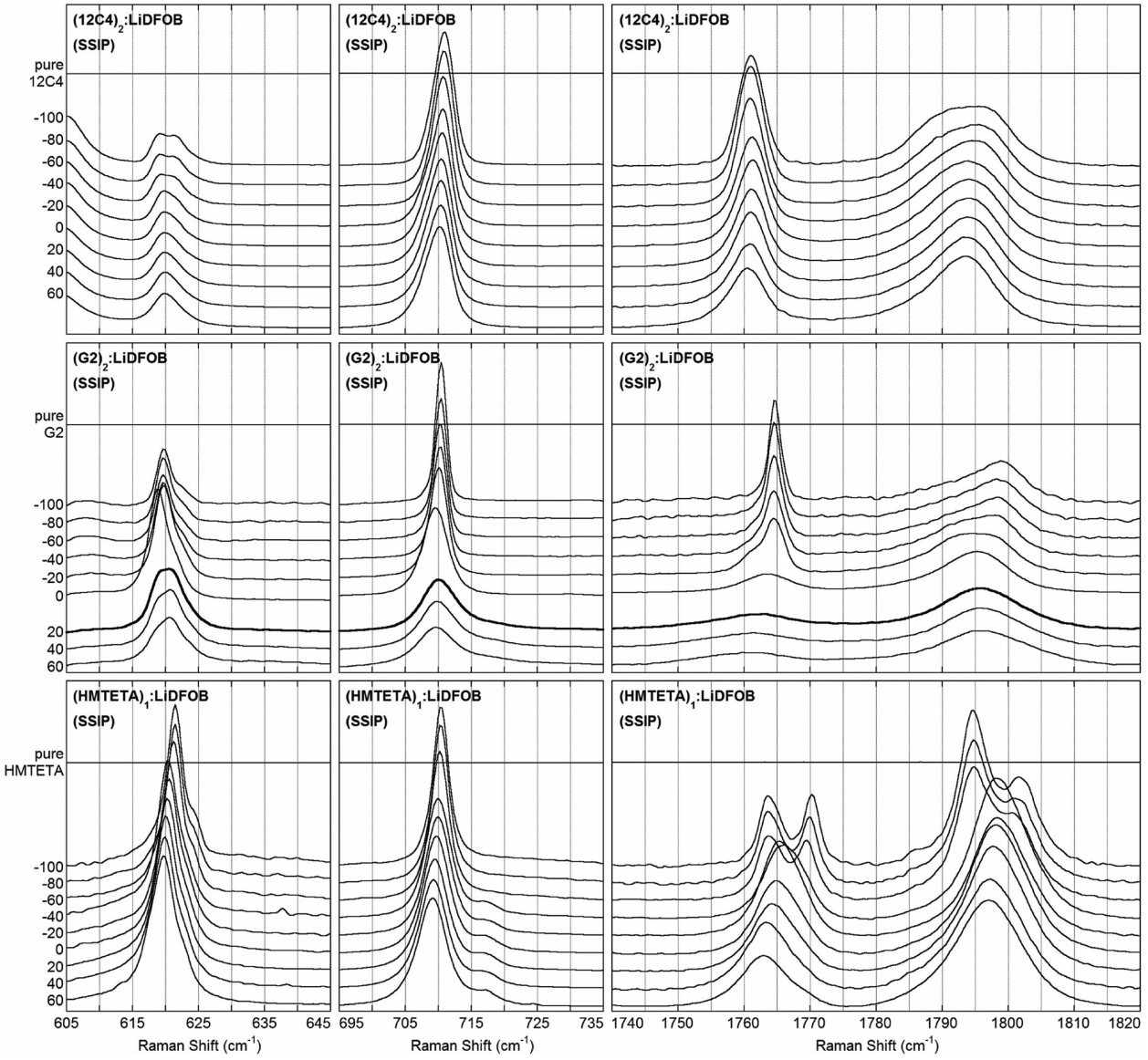

Figure 5. Raman spectra of the $DFOB^-$ anion vibrational band variation for the (speculative) SSIP crystalline solvates: $(12C4)_2$:LiDFOB, $(G2)_2$:LiDFOB, and $(HMTETA)_1$:LiDFOB (bold spectra indicate that the solvate has melted at this temperature).

were therefore analyzed in depth. Representative data are shown in Figures 5 and 6. The remaining sets of data are provided in the SI. A summary of the 705−725 cm^{-1} results for the $DFOB^-$ anion Raman band positions as a function of temperature for the crystalline LiDFOB solvates is shown in Figure 7.

The data in Figure 5 are for speculative SSIP solvates as no crystal structures are yet known for a SSIP solvate with LiDFOB. Attempts were made to determine the crystal structures of the $(12C4)_2$:LiDFOB, $(G2)_2$:LiDFOB, and $(HMTETA)_1$:LiDFOB solvates, but these efforts were unsuccessful due to the very energetic solid−solid phase transitions which occur for these solvates at low temperature (SI) and the presence of significant disorder within the solvate structures in the higher temperature phases. There are no reported crystal structures yet known for solvates with HMTETA and LiX salts, but $(12C4)_2$:LiX[63−67] and $(G2)_2$:LiX[50,68−71] solvates are well-known—all of which have uncoordinated anions (i.e., SSIP solvates). The band positioned near 710 cm^{-1} for all three speculative SSIP solvates remains relatively fixed over the entire temperature range (Figures 5 and 7). In contrast, multiple bands are present near 620 cm^{-1} which differ for the three solvates, as do the bands near 1760 and 1800 cm^{-1} (Figure 5).

The data in Figure 6 correspond to the CIP solvates with known crystal structures. There is rather poor conformity in the band positions for all three regions of the spectra for these solvates. The symmetric C═O band near 1800 cm^{-1} (1906 cm^{-1} from the calculations) also includes the C−O bonds (Chart 3). A comparison of the bond lengths/angles for the CIP-I anions (SI) suggests that these have a very similar geometry. If the bands near 1760 and 1796 cm^{-1} in the spectrum for the $(Et\text{-}G1)_{3/2}$:LiDFOB solvate correspond to the CIP-I anion (rather than the CIP-II anion), then there is very good agreement with the same bands in the $(TMS)_2$:LiDFOB spectrum (Figure 6), but there is then poor agreement between the solvates for the bands near 620 cm^{-1} and 710 cm^{-1} (Figure 6).

The summary of the data for the ring breathing vibrational mode near 710 cm^{-1} shown in Figure 7 suggests that it will be

dx.doi.org/10.1021/jp309102c | J. Phys. Chem. C 2013, 117, 5521−5531

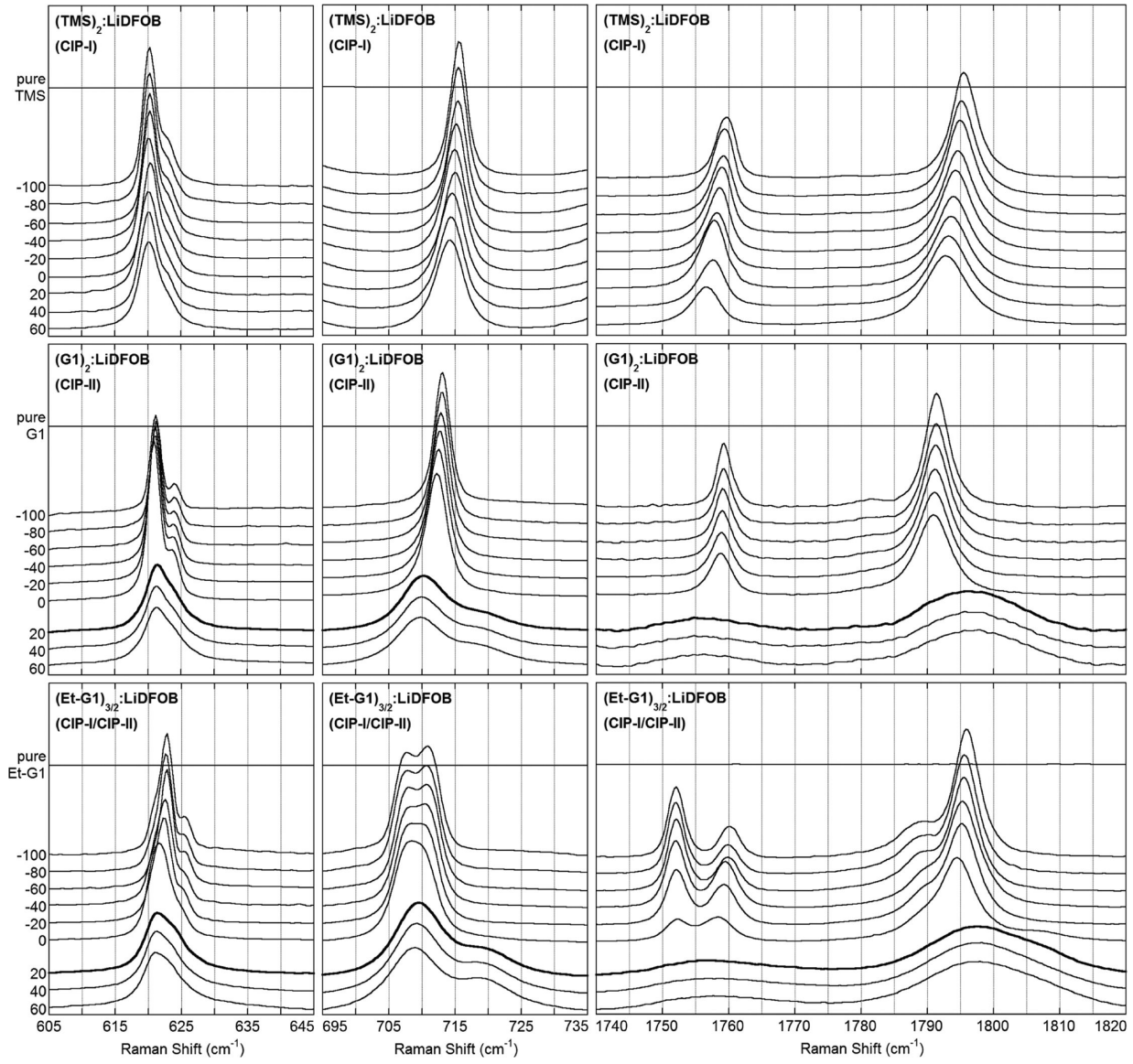

Figure 6. Raman spectra of the $DFOB^-$ anion vibrational band variation for the CIP crystalline solvates: $(TMS)_2$:LiDFOB, $(G1)_2$:LiDFOB and $(Et\text{-}G1)_{3/2}$:LiDFOB (bold spectra indicate that the solvate has melted at this temperature).

quite difficult to accurately deconvolute the complex spectra for the $DFOB^-$ anion in the liquid phase to identify specific anion interactions. This is due to both the numerous forms of $DFOB^-$...Li^+ cation coordination which are possible and the variability in the band positions for any given form of anion coordination. This latter point is particularly true for the AGG solvates which have considerable variability in the anion geometry (SI). Given that each of the anion bands originates from the combination of multiple vibrations (Chart 3), it is not surprising that the anion geometry variation results in widely different spectra. In general, however, the band positions in the 710−725 cm^{-1} range, especially when also considering the other regions of the spectra, do provide an indication of the relative fraction of SSIP, CIP, and AGG solvates (Figure 7). For example, upon melting, notable changes in the spectra occur for the $(G1)_2$:LiDFOB and $(Et\text{-}G1)_{3/2}$:LiDFOB solvates (Figure 6). The spectra, which bear a close resemblance to the spectra for the melted $(G2)_2$:LiDFOB solvate, suggest that the liquid melts obtained from the crystalline CIP solvates likely consist of a significant fraction of SSIP solvates (in addition to CIP solvates) with a lesser amount of AGG-I and perhaps AGG-II solvates. This is quite interesting given that melting of solvates often results in increased association (desolvation) of the solvate species rather than increased solvation (i.e., formation of SSIP solvates).[40,41]

Other forms of $DFOB^-$...Li^+ cation coordination than those found in the crystalline solvates (i.e., Chart 1) are possible/plausible in liquid electrolytes. DFT calculations identified five distinct CIP forms of coordination as energy minima (A−E, Chart 4), but only the LiDFOB-A ion pair was found to be strongly energetically favored for all four calculation methods employed (Table 2). Furthermore, as this type of bidentate $DFOB^-$ coordination via the carbonyl oxygen atoms is found in many of the crystalline solvates, as noted above, both the computational and experimental results suggest that there is a strong preference for this type of coordination. The vibrational modes for the LiDFOB-A ion pair are given in the SI, along with the Gaussian 09 output file for this ion pair.

dx.doi.org/10.1021/jp309102c | J. Phys. Chem. C 2013, 117, 5521−5531

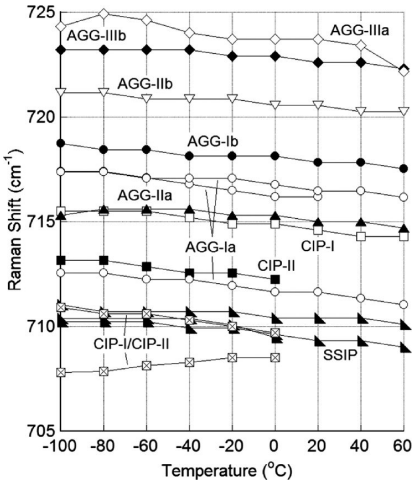

Figure 7. Summary of the Raman band peak position for the $DFOB^-$ anion ring breathing vibrational band for various crystalline solvates (see SI for the assignments of the data to specific solvates).

Chart 4. Stable Ion Pairs Obtained for LiDFOB from DFT Calculations[a]

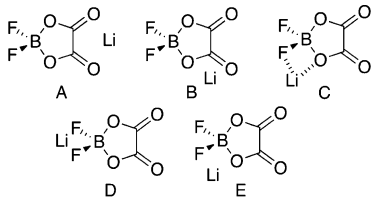

[a]While C and E look the same superficially, C has the Li^+ cation in the FBO plane and E has the cation in the oxalate plane.

Table 2. Energies of the Calculated Ion-Pairs (Relative to LiDFOB-A)

MO6−2X	ΔE (kJ mol^{-1})	B3LYP	ΔE (kJ mol^{-1})
LiDFOB-A	0.0	LiDFOB-A	0.0
LiDFOB-B	60.4	LiDFOB-B	59.5
LiDFOB-C	51.0	LiDFOB-C	52.2
LiDFOB-D	52.2	LiDFOB-D	51.6
LiDFOB-E	62.6	LiDFOB-E	65.1
MO6−2X-SMD	ΔE (kJ mol^{-1})	B3LYP-SMD	ΔE (kJ mol^{-1})
LiDFOB-A	0.0	LiDFOB-A	0.0
LiDFOB-B	33.5	LiDFOB-B	22.7
LiDFOB-C	32.5	LiDFOB-C	35.9
LiDFOB-D	28.4	LiDFOB-D	28.0
LiDFOB-E	38.1	LiDFOB-E	37.4

4. CONCLUSIONS

Numerous crystal structures of LiDFOB solvates are reported which provide significant insight into the manner in which the $DFOB^-$ anion coordinates Li^+ cations. These solvates have been extensively characterized with Raman spectroscopy to link the vibrational bands with specific forms of $DFOB^-$...Li^+ cation coordination. This work has been complemented with DFT calculations to identify the origin (vibrational modes) of the $DFOB^-$ anion vibrational bands.

■ ASSOCIATED CONTENT

Supporting Information

Gaussian file for the $DFOB^-$ anion and LiDFOB-A ion pair to visualize anion vibrational modes; calculated Raman/IR vibrational information for the LiDFOB-A ion pair; differential scanning calorimetry (DSC) heating traces for the solvates; tables of bond lengths and angles for the CIP and AGG solvates; full Raman spectra for the AGG solvates; ion packing diagrams, additional details of the structure determination and crystallographic data (PDF) and crystallographic information files (CIFs) for the crystalline solvate structures (CIFs may be readily viewed with freeware programs such as Mercury or Jmol). This material is available free of charge via the Internet at http://pubs.acs.org.

■ AUTHOR INFORMATION

Corresponding Author

*Tel: 919-513-2917. E-mail: whender@ncsu.edu.

Notes

The authors declare no competing financial interests.

■ ACKNOWLEDGMENTS

The authors wish to express their gratitude to the U.S. Department of Energy (DOE) Batteries for Advanced Transportation Technologies (BATT) Program which fully supported the experimental portion of this research under Award No. DE-AC02-05-CH11231. The Swedish Energy Agency is acknowledged for funding the computation portion of this research via a VR/STEM grant and SNIC for the allocation of computational resources. The authors also wish to thank the Department of Chemistry of North Carolina State University and the State of North Carolina for funding the purchase of the Apex2 diffractometer.

■ REFERENCES

(1) Tsujioka, S.; Takase, H.; Takahashi, M.; Sugimoto, H.; Koide, M. *Electrolyte for Electrochemical Device*. US Patent 6,506,516 B1, 2003 (filed: June 7, 1999).

(2) Zhang, S. S. An Unique Lithium Salt for the Improved Electrolyte of Li-Ion Battery. *Electrochem. Commun.* **2006**, *8*, 1423−1428.

(3) Zhou, H.; Liu, F.; Li, J. Preparation, Thermal Stability and Electrochemical Properties of LiODFB. *Appl. Mech. Mater.* **2012**, *152−154*, 1106−1111.

(4) Yang, C.; Ren, Y.; Wu, B.; Wu, F. Formulation of a New Type of Electrolytes for $LiNi_{1/3}Co_{1/3}Mn_{1/3}O_2$ Cathodes Working in an Ultra-Low Temperature Range. *Adv. Mater. Res.* **2012**, *455−456*, 258−264.

(5) Aravindan, V.; Vickaman, P. Effect of Aging on the Ionic Conductivity of Polyvinylidenefluoride−Hexafluoropropylene (PVdF−HFP) Membrane Impregnated with Different Lithium Salts. *Ind. J. Phys.* **2012**, *86*, 341−344.

(6) Hu, M.; Wei, J.; Xing, L.; Zhou, Z. Effect of Lithium Difluoro(oxalate) borate (LiDFOB) Additive on the Performance of High-Voltage Lithium-Ion Batteries. *J. Appl. Electrochem.* **2012**, *42*, 291−296.

(7) Dalavi, S.; Guduru, P.; Lucht, B. L. Performance Enhancing Electrolyte Additives for Lithium Ion Batteries with Silicon Anodes. *J. Electrochem. Soc.* **2012**, *159*, A642−A646.

(8) Wu, X.; Wang, Z.; Li, X.; Guo, H.; Zhang, Y.; Xiao, W. Effect of Lithium Difluoro(oxalato)borate and Heptamethyldisilazane with Different Concentrations on Cycling Performance of $LiMn_2O_4$. *J. Power Sources* **2012**, *204*, 133−138.

(9) Aravindan, V.; Gnanaraj, J.; Madhavi, S.; Liu, H.-K. Lithium-Ion Conducting Electrolyte Salts for Lithium Batteries. *Chem.—Eur. J.* **2011**, *17*, 14326−14346.

(10) Li, S.; Xu, X.; Shi, X.; Cui, X. Electrochemical Performance of Lithium Difluoro(oxalate)borate Synthesized by a Novel Method. *Adv. Mater. Res.* **2011**, *197*−*198*, 1121−1124.
(11) Allen, J. L.; Han, S.-D.; Boyle, P. D.; Henderson, W. A. Crystal Structure and Physical Properties of Lithium Difluoro(oxalato)borate (LiDFOB or $LiBF_2O_x$). *J. Power Sources* **2011**, *196*, 9737−9742.
(12) Zugmann, S.; Fleischmann, M.; Amereller, M.; Gschwind, R. M.; Winter, M.; Gores, H. J. Salt Diffusion Coefficients, Concentration Dependence of Cell Potentials, and Transference Numbers of Lithium Difluoromono(oxalato)borate-Based Solutions. *J. Chem. Eng. Data* **2011**, *56*, 4786−4789.
(13) Zugmann, S.; Fleischmann, M.; Amereller, M.; Gschwind, R. M.; Wiemhöfer, H. D.; Gores, H. J. Measurement of Transference Numbers for Lithium Ion Electrolytes via Four Different Methods, a Comparative Study. *Electrochim. Acta* **2011**, *56*, 3926−3933.
(14) Zhou, L.; Li, W.; Xu, M.; Lucht, B. Investigation of the Disproportionation Reactions and Equilibrium of Lithium Difluoro(oxalato) Borate (LiDFOB). *Electrochem. Solid-State Lett.* **2011**, *14*, A161−A164.
(15) Zugmann, S.; Moosbauer, D.; Amereller, M.; Schreiner, C.; Wudy, F.; Schmitz, R.; Schmitz, R.; Isken, P.; Dippel, C.; Müller, R.; et al. Electrochemical Characterization of Electrolytes for Lithium-Ion Batteries Based on Lithium Difluoromono(oxalato)borate. *J. Power Sources* **2011**, *196*, 1417−1424.
(16) Allen, J. L.; Boyle, P. D.; Henderson, W. A. Lithium Difluoro(oxalato)borate Tetramethylene Sulfone Disolvate. *Acta Crystallogr.* **2011**, *E67*, m533.
(17) Amine, K.; Chen, Z.; Zhang, Z.; Liu, J.; Lu, W.; Qin, Y.; Lu, J.; Curtis, L.; Sun, Y.-K. Mechanism of Capacity Fade of MCMB/$Li_{1.1}[Ni_{1/3}Mn_{1/3}Co_{1/3}]_{0.9}O_2$ Cell at Elevated Temperature and Additives to Improve Its Cycle Life. *J. Mater. Chem.* **2011**, *21*, 17754−17759.
(18) Xu, M.; Zhou, L.; Hao, L.; Xing, L.; Li, W.; Lucht, B. L. Investigation and Application of Lithium Difluoro(oxalate)borate (LiDFOB) as Additive to Improve the Thermal Stability of Electrolyte for Lithium-Ion Batteries. *J. Power Sources* **2011**, *196*, 6794−6801.
(19) Yang, L.; Markmaitree, T.; Lucht, B. L. Inorganic Additives for Passivation of High Voltage Cathode Materials. *J. Power Sources* **2011**, *196*, 2251−2254.
(20) Zygadło-Monikowska, E.; Florjańczyk, Z.; Kubisa, P.; Biedroń, T.; Tomaszewska, A.; Ostrowska, J.; Langwald, N. Mixture of $LiBF_4$ and Lithium Difluoro(oxalato)borate for Application as a New Electrolyte for Lithium-Ion Batteries. *J. Power Sources* **2010**, *195*, 6202−6206.
(21) Zhang, Z.; Chen, X.; Li, F.; Lai, Y.; Li, J.; Liu, P.; Wang, X. $LiPF_6$ and Lithium Oxalyldifluoroborate Blend Salts Electrolyte for $LiFePO_4$/Artificial Graphite Lithium-Ion Cells. *J. Power Sources* **2010**, *195*, 7397−7402.
(22) Fu, M. H.; Huang, K. L.; Liu, S. Q.; Liu, J. S.; Li, Y. K. Lithium Difluoro(oxalato)borate/Ethylene Carbonate + Propylene Carbonate + Ethyl (Methyl) Carbonate Electrolyte for $LiMn_2O_4$ Cathode. *J. Power Sources* **2010**, *195*, 862−866.
(23) Li, J.; Xie, K.; Lai, Y.; Zhang, Z.; Li, F.; Hao, X.; Chen, X.; Liu, Y. Lithium Oxalyldifluoroborate/Carbonate Electrolytes for $LiFePO_4$/Artificial Graphite Lithium-Ion Cells. *J. Power Sources* **2010**, *195*, 5344−5350.
(24) Moosbauer, D.; Zugmann, S.; Amereller, M.; Gores, H. J. Effect of Ionic Liquids as Additives on Lithium Electrolytes: Conductivity, Electrochemical Stability, and Aluminum Corrosion. *J. Chem. Eng. Data* **2010**, *55*, 1794−1798.
(25) Huang, J.; Fan, L.-Z.; Yu, B.; Xing, T.; Qiu, W. Density Functional Theory Studies on the B-Containing Lithium Salts. *Ionics* **2010**, *16*, 509−513.
(26) Aravindan, V.; Vickraman, P.; Krishnaraj, K. Li^+ Ion Conduction in TiO_2 Filled Polyvinylidenefluoride-co-hexafluoropropylene Based Novel Nanocomposite Polymer Electrolyte Membranes with LiDFOB. *Curr. Appl Phys.* **2009**, *9*, 1474−1479.
(27) Amereller, M.; Multerer, M.; Schreiner, C.; Lodermeyer, J.; Schmid, A.; Barthel, J.; Gores, H. J. Investigation of the Hydrolysis of Lithium Bis[1,2-oxalato(2-)-*O*,*O*′] Borate (LiBOB) in Water and Acetonitrile by Conductivity and NMR Measurements in Comparison to Some Other Borates. *J. Chem. Eng. Data* **2009**, *54*, 468−471.
(28) Xiao, A.; Yang, L.; Lucht, B. L.; Kang, S.-H.; Abraham, D. P. Examining the Solid Electrolyte Interphase on Binder-Free Graphite Electrodes. *J. Electrochem. Soc.* **2009**, *156*, A318−A327.
(29) Chen, Z.; Qin, Y.; Liu, J.; Amine, K. Lithium Difluoro(oxalato)-borate as Additive to Improve the Thermal Stability of Lithiated Graphite. *Electrochem. Solid-State Lett.* **2009**, *12*, A69−A72.
(30) Gao, H.-Q.; Zhang, Z.-A.; Lai, Y.-Q.; Li, J.; Liu, Y.-X. Structure Characterization and Electrochemical Properties of New Lithium Salt LiODFB for Electrolyte of Lithium Ion Batteries. *J. Cent. South Univ. Technol.* **2008**, *15*, 830−834.
(31) Aravindan, V.; Vickraman, P.; Krishnaraj, K. Lithium Difluoro-(oxalate)borate-Based Novel Nanocomposite Polymer Electrolytes for Lithium Ion Batteries. *Polym. Int.* **2008**, *57*, 932−938.
(32) Kang, S.-H.; Abraham, D. P.; Xiao, A.; Lucht, B. L. Investigating the Solid Electrolyte Interphase Using Binder-Free Graphite Electrodes. *J. Power Sources* **2008**, *175*, 526−532.
(33) Abraham, D. P.; Furczon, M. M.; Kang, S.-H.; Dees, D. W.; Jansen, A. N. Effect of Electrolyte Composition on Initial Cycling and Impedance Characteristics of Lithium-Ion Cells. *J. Power Sources* **2008**, *180*, 612−620.
(34) Chen, Z.; Liu, J.; Amine, K. Lithium Difluoro(oxalato)borate as Salt for Lithium-Ion Batteries. *Electrochem. Solid-State Lett.* **2007**, *10*, A45−A47.
(35) Zhang, S. S. Electrochemical Study of the Formation of a Solid Electrolyte Interface on Graphite in a $LiBC_2O_4F_2$-Based Electrolyte. *J. Power Sources* **2007**, *163*, 713−718.
(36) Aravindan, V.; Vickraman, P. A Novel Gel Electrolyte with Lithium Difluoro(oxalato)borate Salt and Sb_2O_3 Nanoparticles for Lithium Ion Batteries. *Solid State Sci.* **2007**, *9*, 1069−1073.
(37) Liu, J.; Chen, Z.; Busking, S.; Amine, K. Lithium Difluoro-(oxalato)borate as a Functional Additive for Lithium-Ion Batteries. *Electrochem. Commun.* **2007**, *9*, 475−479.
(38) Liu, J.; Chen, Z.; Busking, S.; Belharouak, I.; Amine, K. Effect of Electrolyte Additives in Improving the Cycle and Calendar Life of Graphite/$Li_{1.1}[Ni_{1/3}Co_{1/3}Mn_{1/3}]_{0.9}O_2$ Li-Ion Cells. *J. Power Sources* **2007**, *174*, 852−855.
(39) Zhang, S. S. A Review on Electrolyte Additives for Lithium-Ion Batteries. *J. Power Sources* **2006**, *162*, 1379−1394.
(40) Seo, D. M.; Borodin, O.; Han, S.-D.; Ly, Q.; Boyle, P. D.; Henderson, W. A. Electrolyte Solvation and Ionic Association I. Acetonitrile-Lithium Salt Mixtures: Intermediate and Highly Associated Salts. *J. Electrochem. Soc.* **2012**, *159*, A553−A565.
(41) Seo, D. M.; Borodin, O.; Han, S.-D.; Boyle, P. D.; Henderson, W. A. Electrolyte Solvation and Ionic Association II. Acetonitrile-Lithium Salt Mixtures: Highly Dissociated Salts. *J. Electrochem. Soc.* **2012**, *159*, A1489−A1500.
(42) Huang, W.; Frech, R.; Wheeler, R. A. Molecular Structures and Normal Vibrations of Trifluoromethane Sulfonate ($CF_3SO_3^-$) and Its Lithium Ion Pairs and Aggregates. *J. Phys. Chem.* **1994**, *98*, 100−110.
(43) Gejji, S. P.; Suresh, C. H.; Babu, K.; Gadre, S. R. Ab Initio Structure and Vibrational Frequencies of $(CF_3SO_2)_2N^-Li^+$ Ion Pairs. *J. Phys. Chem. A* **1999**, *103*, 7474−7480.
(44) Holomb, R.; Xu, W.; Markusson, H.; Johansson, P.; Jacobsson, P. Vibrational Spectroscopy and Ab Initio Studies of Lithium Bis(oxalato)borate (LiBOB) in Different Solvents. *J. Phys. Chem. A* **2006**, *110*, 11467−11472.
(45) Scheers, J.; Niedzicki, L.; Zukowska, G. Z.; Johansson, P.; Wieczorek, W.; Jacobsson, P. Ion−Ion and Ion−Solvent Interactions in Lithium Imidazolide Electrolytes Studied by Raman Spectroscopy and DFT Models. *Phys. Chem. Chem. Phys.* **2011**, *13*, 11136−11147.
(46) Johansson, P.; Béranger, S.; Armand, M.; Nilsson, H.; Jacobsson, P. Spectroscopic and Theoretical Study of the 1,2,3-Triazole-4,5-dicarbonitrile Anion and Its Lithium Ion Pairs. *Solid State Ionics* **2003**, *156*, 129−139.
(47) Grondin, J.; Talaga, D.; Lassègues, J.-C.; Henderson, W. A. Raman Study of Crystalline Solvates Between Glymes

$CH_3(OCH_2CH_2)_nOCH_3$ (n = 1, 2 and 3) and $LiClO_4$. *Phys. Chem. Chem. Phys.* **2004**, *6*, 938−944.
(48) Grondin, J.; Lassègues, J.-C.; Chami, M.; Servant, L.; Talaga, D.; Henderson, W. A. Raman Study of Tetraglyme−$LiClO_4$ Solvate Structures. *Phys. Chem. Chem. Phys.* **2004**, *6*, 4260−4267.
(49) Henderson, W. A.; Brooks, N. R. Crystals from Concentrated Glyme Mixtures. The Single-Crystal Structure of $LiClO_4$. *Inorg. Chem.* **2003**, *42*, 4522−4524.
(50) Henderson, W. A.; Brooks, N. R.; Brennessel, W. W.; Young, V. G., Jr. $LiClO_4$ Electrolyte Solvate Structures. *J. Phys. Chem. A* **2004**, *108*, 225−229.
(51) Henderson, W. A.; Brooks, N. R.; Brennessel, W. W.; Young, V. G., Jr. Triglyme−Li^+ Cation Solvate Structures: Models for Amorphous Concentrated Liquid and Polymer Electrolytes (I). *Chem. Mater.* **2003**, *15*, 4679−4684.
(52) Henderson, W. A.; Brooks, N. R.; Young, V. G., Jr. Tetraglyme−Li^+ Cation Solvate Structures: Models for Amorphous Concentrated Liquid and Polymer Electrolytes (II). *Chem. Mater.* **2003**, *15*, 4685−4690.
(53) *SAINT and SADABS*; Bruker AXS Inc.: Madison, WI, , 2009.
(54) Altomare, A.; Cascarano, G.; Giacovazzo, C.; Guagliardi, A.; Burla, M. C.; Polidori, G.; Camalli, M. SIR92—A Program for Automatic Solution of Crystal Structures by Direct Methods. *J. Appl. Crystallogr.* **1994**, *27*, 435−436.
(55) *Bruker-AXS, XL version 2009.9*; Bruker-AXS Inc.: Madison, WI, 2009.
(56) Vosko, S. H.; Wilk, L.; Nusair, M. Accurate Spin-Dependent Electron Liquid Correlation Energies for Local Spin Density Calculations: A Critical Analysis. *Can. J. Phys.* **1980**, *58*, 1200−1211.
(57) Lee, C.; Yang, W.; Parr, R. G. Development of the Colle-Salvetti Conelation Energy Formula into a Functional of the Electron Density. *Phys. Rev. B* **1988**, *37*, 785−789.
(58) Becke, A. D. Density-Functional Thermochemistry. III. The Role of Exact Exchange. *J. Chem. Phys.* **1993**, *98*, 5648−5652.
(59) Zhao, Y.; Truhlar, D. G. The M06 Suite of Density Functionals for Main Group Thermochemistry, Thermochemical Kinetics, Noncovalent Interactions, Excited States, and Transition Elements: Two New Functionals and Systematic Testing of Four M06-Class Functionals and 12 Other Functionals. *Theor. Chem. Acc.* **2008**, *120*, 215−241.
(60) Marenich, A. V.; Cramer, C. J.; Truhlar, D. G. Universal Solvation Model Based on Solute Electron Density and on a Continuum Model of the Solvent Defined by the Bulk Dielectric Constant and Atomic Surface Tensions. *J. Phys. Chem. B* **2009**, *113*, 6378−6396.
(61) Frisch, M. J.; Trucks, G. W.; Schlegel, H. B.; Scuseria, G. E.; Robb, M. A.; Cheeseman, J. R.; Scalmani, G.; Barone, V.; Mennucci, B.; Petersson, G. A. et al. *Gaussian 09, Revision B.01*; Gaussian, Inc.: Wallingford CT, 2010.
(62) Andreev, Y. G.; Seneviratne, V.; Khan, M.; Henderson, W. A.; Frech, R. E.; Bruce, P. G. Crystal Structures of Poly(Ethylene Oxide)$_3$:$LiBF_4$ and (Diglyme)$_n$:$LiBF_4$ (n = 1,2). *Chem. Mater.* **2005**, *17*, 767−772.
(63) Dillon, R. E. A.; Stern, C. L.; Shriver, D. F. Structural Comparisons of Fast Ion Conductors Consisting of $Li[(CF_3SO_2)_2N]$ Complexes with Cryptands or Crown Ether. *Solid State Ionics* **2000**, *133*, 247−255.
(64) Lewis, R. A.; Wu, G.; Hayton, T. W. Stabilizing High-Valent Metal Ions with a Ketimide Ligand Set: Synthesis of $Mn(N{=}C^tBu_2)_4$. *Inorg. Chem.* **2011**, *50*, 4660−4668.
(65) Hope, H.; Olmstead, M. M.; Power, P. P.; Xu, X. X-Ray Crystal Structures of the Diphenylphosphide and Arsenide Anions: Use of a Crown Ether to Effect Complete Metal Cation and Organometalloid Anion Separation. *J. Am. Chem. Soc.* **1984**, *106*, 819−821.
(66) Gallucci, J. C.; Sivik, M. R.; Paquette, L. A.; Zaegel, F.; Meunier, P.; Gautheron, B. Two Derivatives of Lithium Isodicyclopentadienide: [(1,2,3,3a,7a-η)-4,5,6,7-Tetrahydro-4,7-methanoindenido](*N*,*N*,*N*′,*N*′-tetramethylethylenediamine)lithium and Bis(1,4,7,10-tetraoxacyclododecane)lithium(1$^+$) Bis[(1,2,3,3a,7a-η)-4,5,6,7-tetrahydro-4,7-methanoindenido]lithate(1$^-$). *Acta Crystallogr.* **1996**, *C52*, 1673−1679.
(67) Liddle, S. T.; Clegg, W. A Homologous Series of Crown-Ether-Complexed Alkali Metal Amides as Discrete Ion-Pair Species: Synthesis and Structures of [M(12-crown-4)$_2$][PyNPh·PyN(H)Ph] (M = Li, Na and K). *Polyhedron* **2003**, *22*, 3507−3513.
(68) Esterhuysen, M. W.; Raubenheimer, H. G. Lithium [Bis-{benzoyl-$W(CO)_5$}(μ_2-hydrogen)]−A Charge-Assisted H^+-Bridged Organometallic Complex Prepared by Selective Li^+ Ion Replacement. *Eur. J. Inorg. Chem.* **2003**, *2003*, 3861−3869.
(69) Pauls, J.; Iravani, E.; Köhl, P.; Neumüller, B. Metallat-Ionen $[Al(OR)_4]^-$ als Chelatliganden für Übergangsmetall-Kationen. *Z. Anorg. Allg. Chem.* **2004**, *630*, 876−884.
(70) Seneviratne, V.; Frech, R.; Furneaux, J. E.; Khan, M. Characterization of Crystalline and Solution Phases of Diglyme−$LiSbF_6$. *J. Phys. Chem. B* **2004**, *108*, 8124−8128.
(71) Palitzsch, W.; Böhme, U.; Beyer, C.; Roewer, G. First Crystal Structure of a Cyclohexasilyl Transition-Metal Derivative, $[(DIME)_2Li][Mo(CO)_5Si_6Me_{11}]$ (DIME = Diethylene Glycol Dimethyl Ether). *Organometallics* **1998**, *17*, 2965−2969.